Acquiring and Processing Light Deflection Maps for Transparent Object Inspection

Johannes Meyer
Karlsruhe Institute of Technology KIT
Vision and Fusion Laboratory
Karlsruhe, Germany
https://www.meyer-research.de

Thomas Längle and Jürgen Beyerer
Fraunhofer-Institute of Optronics,
System Technologies and
Image Exploitation IOSB
Karlsruhe, Germany

***Abstract*—Transparent objects play important roles in different sectors, e.g., they are employed in high precision optical systems or to guide laser beams in surgery. Hence, transparent materials have to meet high quality requirements. However, most of the existing elaborated automated inspection approaches are not applicable for the inspection of transparent materials—especially with respect to scattering inhomogeneities. Scattering material defects mainly cause a deflection of incident light rays away from their original optical path. This article proposes a novel optical system based on a transmission-type laser scanner that acquires so-called deflection maps of transparent objects. By means of two subsequent processing methods—one based on a spatial gradient calculation, the other relying on vector analysis—scattering material defects can be visualized even in test objects with a complex 3D-shape. Experiments performed using a first prototype and different test objects approve the proposed approach.**

I. Introduction

The automated visual inspection of transparent objects and materials is a challenging task. Many elaborated machine vision methods require the object under test to have a Lambertian surface, i.e., to be diffusely reflecting. This is why these methods can in general not be applied to transparent objects. Transparent materials play important roles in many different kinds of applications. They are employed as windshields, as containers for food and beverages and as high precision optical elements. Transparent components can be affected by various kinds of defects: the material can be contaminated with absorbing or scattering impurities (e.g., particles), the material's index of refraction can vary spatially and also the 3D-geometry of the object can differ from the intended shape. The mentioned fields of application already make clear, that components made of transparent materials have to meet high quality criteria and therefore have to be visually inspected for defects after their production. Since the visual inspection of transparent objects by human workers is fatiguing and error-prone task, much effort has been spent in developing automated inspection systems.

There exist robust and approved concepts for finding absorbing contaminants, inhomogeneities of the index of refraction and shape anomalies in transparent objects [1]. There are also approaches for visualizing scattering impurities (e.g., enclosed air bubbles) in transparent materials [2], however, they are not reliable for objects having a more complex 3D-shape. This is because scattering defects mainly result in a widening or deflection of incident light rays and the object's 3D-shape also leads to light rays being deflected away from their original optical path.

Figure 1 visualizes the macroscopic influences on the deflection of incident light rays, i.e., how the deflection angle changes because of both scattering material defects and the 3D-shape of the test object. For defect-free regions of the test object, the spatial characteristics of the deflection angles of light rays exiting the object show only slight variations. In contrast, around the boundaries of the defect, the exiting light rays are deflected in various directions. Furthermore,

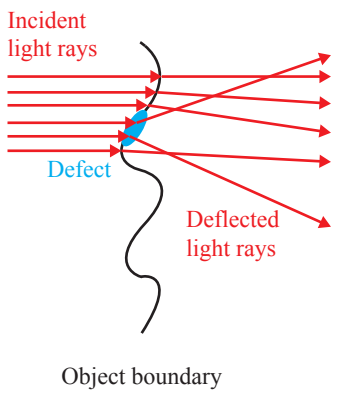

Fig. 1. Macroscopic influence of scattering defects on incident light rays: the 3D-shape of the transparent object causes slight variations in the deflection angle of exiting light rays. In contrast, in a local neighborhood around the boundary of a scattering defect, there are great discontinuities of the deflection direction.

there are also microscopic influences, i.e., certain physical effects, that have to be taken into account. Depending on the geometric dimensions of the defect and on the wavelength of the employed illuminating light, the theories of classical scattering, Mie scattering or even Rayleigh scattering have to be respected [3], [4]. For the detection of material defects, the widening of incident light beams caused by scattering defects as shown in Fig. 2 is of major importance.

This contribution introduces a novel optical setup that allows to capture so-called light deflection maps from transparent objects. In addition, the article proposes subsequent image

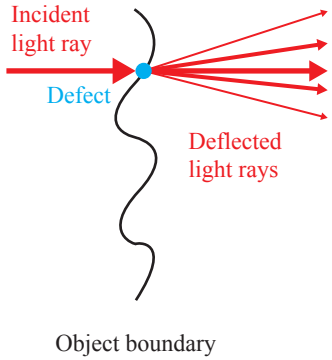

Fig. 2. Microscopic influence of scattering defects on incident light rays: due to different physical effects, light rays that hit a scattering defect that is small with respect to the diameter of the light ray are spread and deflected into multiple directions.

processing methods that yield adequate features for detecting scattering impurities present in the test object.

The article is organized as follows: Section II lists and shortly summarizes related work performed by other researches. In Sec. III, the optical setup of the introduced laser scanner system is shown and explained. Section IV proposes several approaches for extracting features out of the acquired deflection maps that are suitable for detecting scattering material defects. The following Sec. V provides information about a first early prototype and Sec. VI describes and discusses the performed experiments using that prototype. Finally, Sec. VII closes the article with a short summary and a comment on planned future work.

II. Related work

To the knowledge of the authors, there are two groups of researchers that are working on the field of inspecting transparent objects by investigating the distribution of the deflection directions of light rays exiting the test object.

Sudhakar et al. [5] proposed an approach based on a schlieren imaging system. They illuminate the transparent test object with bundles of parallel light rays which are tilted with respect to the optical axis. By placing a spatial light modulator in the focal plane of a lens, they are able to control the tilt angle of the light beams and to simultaneously emit several beams that are tilted by different angles. The transparent test object is observed from its other side with a telecentric camera system. Due to the telecentric stop, only those light rays that propagate parallel to the optical axis after exiting the test object can reach the image sensor. Since the tilt angles of the illuminating light beams are known, spatially resolved deflection maps of the test object can be calculated by capturing an image series for different tilt angles. For every object point, the deflection maps hold the distribution of angles by which light rays get deflected when passing the test object at the respective position. The authors employed the obtained deflection maps to infer the local optical power of contact lenses but they did not use them to detect material defects.

The group of Meyer et al. [6] propose a novel optical setup of a light field camera that is based on a $4f$-system. In concert with a collimated illuminating light beam, this system is able to capture spatially resolved deflection maps by acquiring a single image only. In the system's sensing part, two main lenses are arranged so that they share a common focal plane. A micro lens array is placed in the focal plane of the rear lens and the sensor resides in the focal plane of the micro lens array. By this means, rays that get deflected at different spatial positions inside the measurement field but by the same angle, will hit the sensor at the same position relative to the respective micro lens. The authors show that this invariance does not hold for common light field cameras what makes them inapplicable for measuring deflection angles. After normalizing the deflection maps to so-called histograms of ray deflections (HORDs), Meyer et al. propose to calculate the earth mover's distance between spatially adjacent HORDs in order to detect discontinuities of the ray deflection distribution. For evaluation purposes they simulated the optical system using a physically based rendering framework and inspected transparent test objects contaminated with artificial defects. Their proposed approach shows promising results with respect to the detection of scattering impurities in transparent objects, however, the optical system suffers from the classical light field trade-off between spatial and angular resolution.

III. Laser deflection scanner

This section describes the principal idea of the proposed optical system for acquiring light deflection maps of transparent test objects. Figure 3 visualizes the optical setup. The system is based on a transmissive laser scanner setup that illuminates the measurement field with light rays running parallel to the optical axis. By moving the laser source or by deflecting the laser using a polygon mirror motor, the measurement field can be scanned. The system's sensing part consists of a lens or a parabolic mirror having a two-dimensional sensor in its focal plane.

When a light ray gets deflected by an angle α inside the measurement field, its intersection with the sensor will be displaced with respect to the sensor's center by

$$\delta = \tan(\alpha)\, f\,, \tag{1}$$

with f denoting the focal length of the lens or the parabolic mirror respectively. Since the sensor is placed in the lens' focal plane which is the conjugate plane of the measurement field, spatial information of the measurement field is transformed into directional information in the sensor plane. So regardless of their spatial position inside the measurement field, all light rays that get deflected by the same angle will hit the sensor at the same position. This is why it is necessary to retain the spatial information by sequentially scanning the measurement field. By changing the focal length f, the sensitivity, respectively, the measurement range of the system can be adjusted: a greater f increases the sensitivity as the displacement δ corresponding to a deflection angle α will be greater. However, increasing f reduces the measurement range

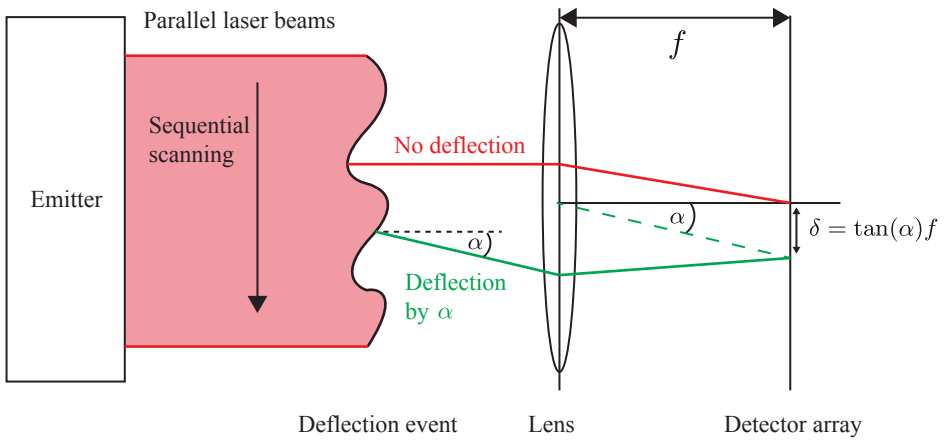

Fig. 3. Principle optical setup of the proposed deflection laser scanner: the test object is illuminated with parallel laser beams. By successively moving the laser source, the test object is spatially scanned. A Fourier lens placed close behind the test object transforms deflections of exiting light rays into spatial displacements on the sensor plane of a detector array.

since the sensor has a limited size and rays being deflected by great angles will miss the sensor.

The data obtained by the laser deflection scanner can be interpreted as deflection maps $L(x, y, \theta, \varphi)$. These maps hold the observed radiance that corresponds to a ray that was emitted at the spatial position $(x, y)^{\mathrm{T}}$ and was deflected inside the measurement field by the azimuthal angle θ and the polar angle φ. In order to account for the discretizations during the sensing process, the mappings

$$x \mapsto m\,, \tag{2}$$
$$y \mapsto n\,, \tag{3}$$
$$\theta \mapsto i\,, \tag{4}$$
$$\varphi \mapsto j\,, \tag{5}$$
$$L(x, y, \theta, \varphi) \mapsto a(m, n, i, j) \tag{6}$$

define the discrete pendants of the continuous quantities x, y, θ, φ and L. For the remaining parts of this article, the term *deflection map* refers to the discretized $a(m, n, i, j)$.

IV. Processing of Deflection Maps

In order to detect scattering defects in transparent materials of which deflection maps $a(m, n, i, j)$ have been acquired, adequate processing steps are needed. As already mentioned in Sec. I, scattering defects result in spatial discontinuities of the deflection direction of the light rays exiting the test object (macroscopic aspect as shown in Fig. 1) or a widening of incident light beams (microscopic aspect as shown in Fig.2).

For some of the further processing steps it is necessary to normalize the angular components of a for every spatial position $(m, n)^{\mathrm{T}}$. This normalized $\tilde{a}$ is obtained via

$$\tilde{a}(m, n, i, j) := \frac{a(m, n, i, j)}{\sum\limits_{(k,l)^{\mathrm{T}}} a(m, n, k, l)}\,. \tag{7}$$

In the following, different approaches for detecting spatial discontinuities in a, respectively, in $\tilde{a}$ will be described.

A. Discontinuity detection by gradient calculation

Classical image processing approaches would calculate a gradient image in order to detect edges, i.e., spatial discontinuities of the gray values. By setting $S(m, n) := \tilde{a}(m, n, \cdot, \cdot)$, a spatial gradient is given by

$$\Delta S(m, n) = \begin{pmatrix} d\left(S(m-1, n), S(m+1, n)\right) \\ d\left(S(m, n-1), S(m, n+1)\right) \end{pmatrix}\,, \tag{8}$$

with $d(\cdot, \cdot)$ denoting a suitable distance measure. Since in the present case, every $S(m, n)$ is a two-dimensional distribution of the respective deflection angles, $d(\cdot, \cdot)$ has to calculate adequate distances. For the detection of scattering defects, $d(\cdot, \cdot)$ should yield high values when there is a great distance between the positions of the peaks of the two deflection distributions and when there is no distinct peak in one of the two deflection distributions. A possible choice for $d(\cdot, \cdot)$ is the so-called earth mover's distance $EMD(\cdot, \cdot)$. In fact, this distance is defined and usually used for comparing two histograms h_1 and h_2 that can also be two-dimensional [7]. Since the $S(m, n)$ contain the normalized deflection maps $\tilde{a}$, the $EMD(\cdot, \cdot)$ can also be employed in the present case. The result of $EMD(h_1, h_2)$ can be interpreted as the minimum costs for transforming h_1 into h_2 or vice versa. For two histograms h_1 and h_2 each having N bins, the earth mover's distance is given by:

$$EMD(h_1, h_2) := \min_{\gamma(k,l) \in \mathcal{M}} \sum_{k=1}^{N} \sum_{l=1}^{N} \gamma(k, l) c(k, l)\,, \tag{9}$$

$$\begin{aligned} \mathcal{M} = \{ & \gamma(k, l) : \gamma(k, l) \geq 0, \\ & \sum_{l} \gamma(k, l) = h_1(k), \\ & \sum_{k} \gamma(k, l) = h_2(l) \}\,, \end{aligned} \tag{10}$$

with $c(k, l)$ denoting the costs of moving one entity from bin k to bin l and with $\gamma(k, l)$ denoting the number of entities transfered from bin k of h_1 to bin l of h_2.

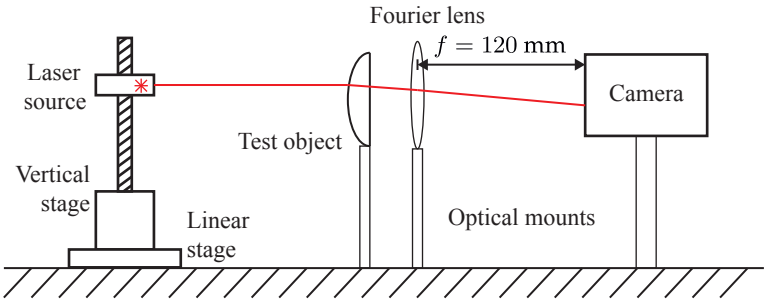

Fig. 4. Schematic layout of the proposed laser deflection scanner prototype.

In order to finally detect present scattering inhomogeneities, the gradient $\|\Delta S(m,n)\|$ can be calculated and common image processing methods can employed, e.g., to find peaks or other abnormalities in $\|\Delta S(m,n)\|$.

B. Analysis of mean deflection directions

As mentioned in the introduction, especially the macroscopic nature of scattering defects in transparent materials is manifested in spatial discontinuities of the main deflection direction. Therefore, another approach for detecting scattering defects is to calculate the mean deflection direction $\bar{\mathbf{r}}(m,n)$ for every spatial position $(m,n)^{\mathrm{T}}$ [6]. As every entry $(i,j)^{\mathrm{T}}$ of $a(m,n,i,j)$ corresponds to a certain deflection direction $\mathbf{r}(i,j)$, the mean deflection direction can be obtained via

$$\bar{\mathbf{r}}(m,n) = \sum_{(i,j)^{\mathrm{T}}} a(m,n,i,j) \cdot \mathbf{r}(i,j)\,. \tag{11}$$

Since the sought-after defects are embedded in $\bar{\mathbf{r}}(m,n)$ as spatial discontinuities, they should lead to great values of the components of the respective Jacobians $\mathbf{J}$ of $\bar{\mathbf{r}}(m,n)$, with

$$\mathbf{J}(m,n) = \begin{pmatrix} \frac{\partial \bar{r}_m}{\partial m}(m,n)\,, & \frac{\partial \bar{r}_m}{\partial n}(m,n) \\ \frac{\partial \bar{r}_n}{\partial m}(m,n)\,, & \frac{\partial \bar{r}_n}{\partial n}(m,n) \end{pmatrix}. \tag{12}$$

In order to detect the spatial discontinuities, a suitable matrix norm $\|\cdot\|$ of $\mathbf{J}$ can be calculated. To emphasize positions with high discontinuities of the mean deflection direction regardless of the actual direction, the Frobenius norm $\|\cdot\|_{\mathrm{F}}$ is a sensible choice [8]. The Frobenius norm of $\mathbf{J}(m,n)$ is obtained via

$$\|\mathbf{J}(m,n)\|_{\mathrm{F}} = \sqrt{\left|\frac{\partial \bar{r}_m}{\partial m}(m,n)\right|^2 + \left|\frac{\partial \bar{r}_m}{\partial n}(m,n)\right|^2 + \left|\frac{\partial \bar{r}_n}{\partial m}(m,n)\right|^2 + \left|\frac{\partial \bar{r}_n}{\partial n}(m,n)\right|^2}. \tag{13}$$

Like for the gradient based methods mentioned before, common image processing methods can be applied to $\|\mathbf{J}(m,n)\|_{\mathrm{F}}$ to find peaks or other abnormalities that might correspond to scattering material defects.

Section VI shows the results of applying the presented processing approaches to acquired deflection maps.

V. A First Prototype

This section describes a first prototype that has been built based on the principle optical setup introduced in Sec. III. The prototype allows to capture deflection maps of small transparent objects that can be used to evaluate the optical setup itself and the processing methods proposed in Sec. IV. The employed parts are all inexpensive standard components that are widely available ensuring that the prototype can easily be rebuilt.

Figure 4 shows the principle setup of the prototype and Fig. 5 shows an actual photograph where the important parts have been extracted. A 650 nm laser diode is attached to a vertical translation stage consisting of a lead screw driven by a stepper motor. The stepper motor is mounted on a Zaber linear translation stage so that together the two translation stages can perform the required two-dimensional scanning. The camera is positioned in the focal plane of the Fourier lens which transforms angular deflections of incident light rays into spatial displacements on the camera sensor. Table I lists the single actually employed components of the described prototype.

TABLE I
Listing of the components used for the described prototype.

Function	Employed component
Laser diode	power: 5 mW, wavelength: 650 nm
Fourier lens	Double-convex, f =120 mm
Camera	JAI SP-20000M-PMCL-F resolution: 3840 x 5120 pixel
Vertical Stage	Bipolar stepper motor with 180 mm lead screw
Linear Stage	Zaber 50 mm travel stage

The two stages and the camera are controlled by a computer. By successively moving the laser source in horizontal and vertical direction and by acquiring a camera image for every step, test object regions of up to 50 mm $\times$ 50 mm can be scanned. This prototype has been used for acquiring the deflection maps in the experiments described in the following section.

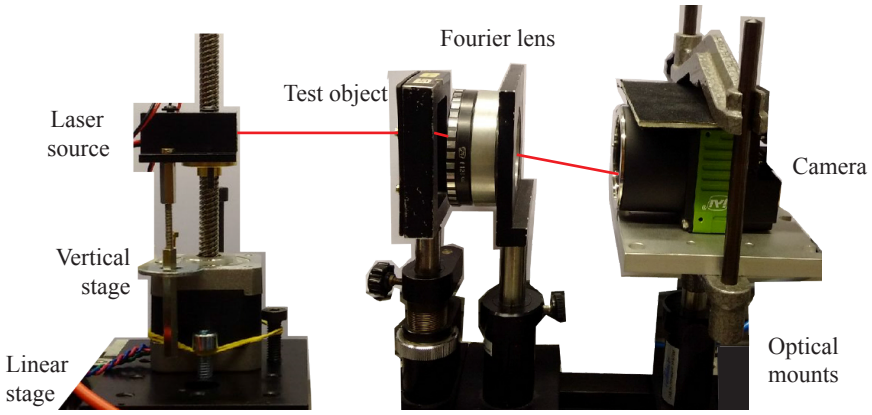

Fig. 5. Photograph showing the extracted components of the built prototype.

VI. Experiments

The prototype described in Sec. V was used in concert with two sorts of test objects in order to evaluate the suitability of the proposed approach for detecting scattering defects in transparent objects. The two kinds of test objects are a cylindrical lens and a double-convex lens both made of glass. Of both kinds, an intact, i.e. a defect-free instance and an instance with scattering surface defects smaller than the laser spot (i.e. with a diameter < 2 mm) were inspected. Deflection maps with a spatial resolution of 39×39 and an angular resolution of 9×9 were acquired[1] for all four test objects. To the acquired deflection maps, the image processing methods introduced in Sec. IV were applied. In the following, the results for the two different kinds of test objects will be discussed. For every inspected test object, the magnitude of the gradient based on the earth mover's distance and the Frobenius norm of the mean deflection directions are calculated and shown as pseudocolor inspection images in Fig. 6.

The inspection images of the double-convex lens show some artifacts at the right-hand boundary. This is because the inspection window was set too close to the boundary of the test object at the respective side, what explains the strong spatial discontinuities of the deflection maps. Aside from that, there is a clear difference between the inspection image corresponding to the defect-free test object instance and that of the defective test object. It is clearly visible that there are scattering defects present in the upper right-hand corner of the test object. However, since the two defects are lying closely to each other, their signatures are connected in the inspection image and they are not distinguishable. Furthermore, there are no important differences between the results of the gradient-based approach and that based on the Frobenius norm of the Jacobians.

The results for the cylindrical lens show clear inspection images for the defect-free test object instance with only slight discontinuities at the boundary of the inspection window. Moreover, the two scattering surface defects are clearly visible and are well separated. In the case of this test object, the approach based on the 2D earth mover's distance seems to be more precise since it suggests that the sizes of the two defects are similar what is actually the case. This cannot be inferred by means of the inspection image obtained using the Frobenius norm of the Jacobians.

In summary, the experiments show that the proposed approach is capable of visualizing scattering defects in transparent materials. However, there still is a great potential for improvements, both considering the optical and mechanical setup and the image processing methods.

[1]Indeed, a much higher angular resolution could have been achieved with the employed camera—however, because of the low precision of the other components, the recorded camera images were downsampled before performing further processing steps.

VII. Summary

The present article showed how scattering material defects inside transparent objects influence incident light rays by deflecting them away from their original optical path. Furthermore, an optical system—a so-called deflection laser scanner—has been proposed, that is able to capture the spatial distribution of the deflection angles of light rays exiting a transparent test object. Two subsequent processing methods have been evaluated that are capable of highlighting scattering defects: One of them is based on a spatial gradient calculation using the earth mover's distance and the other one makes use of the Frobenius norm of the Jacobians of the mean deflection direction. Moreover, the article describes a first prototype realizing the introduced optical setup and shows results of experiments that were conducted using that prototype. The evaluation shows promising results, however, there are still many possibilities for further improvements.

As future work, the authors plan to improve the prototype and the image processing methods. In addition, further histogram comparison methods will be evaluated for the gradient based approach and the authors will evaluate whether it is beneficial to calculate the Jacobians with respect to the whole deflection maps. A more extensive evaluation by inspecting more test objects is also planned as one of the future steps.

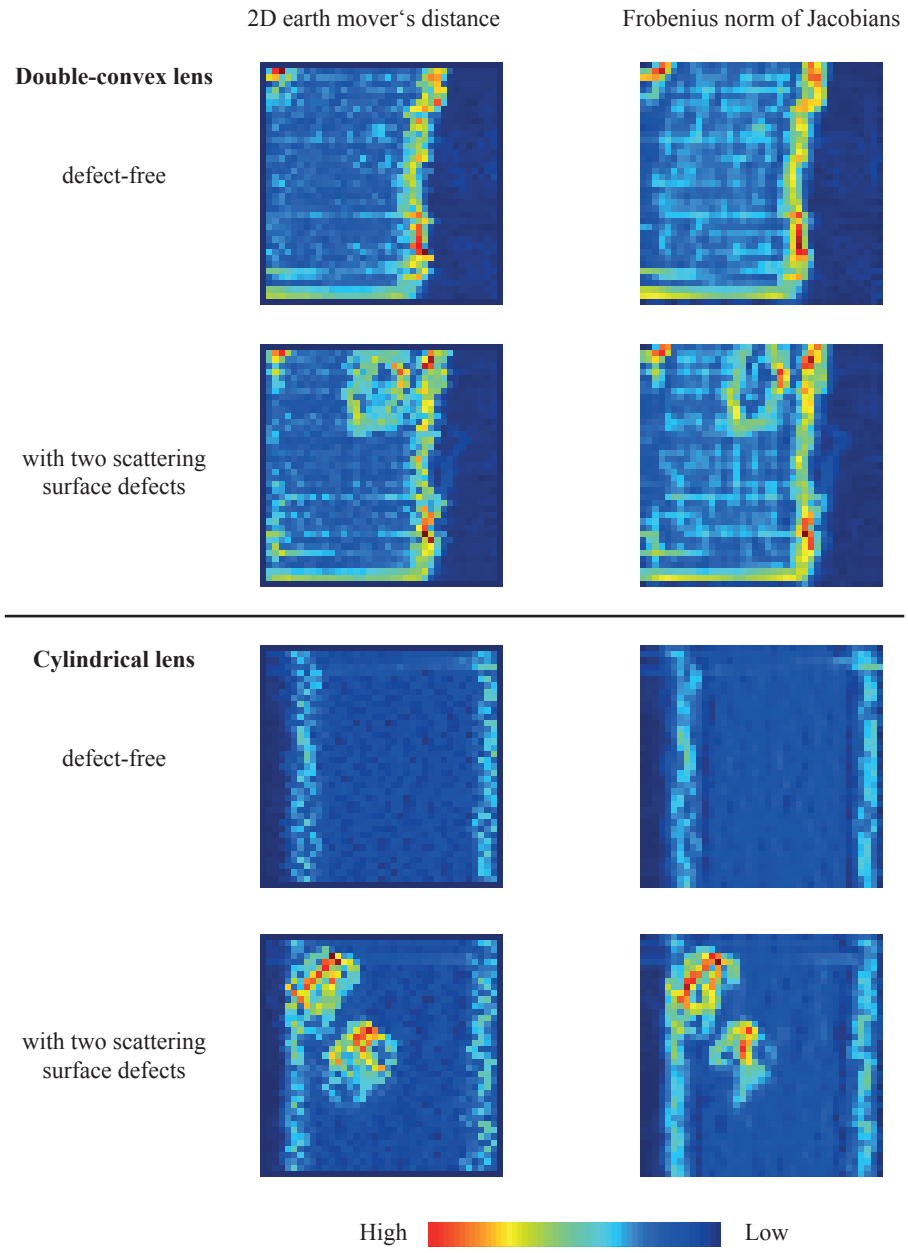

Fig. 6. Pseudocolor images showing the inspection images of four test object instances obtained using the proposed deflection laser scanner prototype and the introduced subsequent processing approaches.

REFERENCES

[1] J. Meyer, “Overview on machine vision methods for finding defects in transparent objects,” Karlsruhe Institute of Technology, Tech. Rep. IES-2015-08, 2015.

[2] M. Hartrumpf and R. Heintz, “Device and method for the classification of transparent components in a material flow,” Patent WO 2009/049594 A1, 2009.

[3] C. F. Bohren and D. R. Huffman, *Absorption and Scattering of Light by Small Particles*. Wiley-VCH Verlag GmbH, 2007.

[4] H. van de Hulst, *Light Scattering by Small Particles*, ser. Dover Books on Physics. Dover Publications, 1957.

[5] P. Sudhakar, L. Jacques, X. Dubois, P. Antoine, and L. Joannes, “Compressive imaging and characterization of sparse light deflection maps,” *SIAM Journal on Imaging Sciences*, vol. 8, no. 3, pp. 1824–1856, 2015.

[6] J. Meyer, T. Längle, and J. Beyerer, “About the acquisition and processing of ray deflection histograms for transparent object inspection,” in *IRISH MACHINE VISION & IMAGE PROCESSING Conference proceedings*, 2016.

[7] Y. Rubner, C. Tomasi, and L. Guibas, “A metric for distributions with applications to image databases,” in *Computer Vision, 1998. Sixth International Conference on*. IEEE, 1998, pp. 59–66.

[8] R. Horn and C. Johnson, *Matrix analysis*. Cambridge University Press, 2012.